journal

J. Am. Ceram. Soc., 1–7 (2016)
DOI: 10.1111/jace.14443

Structural Evolution in Hollandite Solid Solutions Across the A-site Compositional Range from $Ba_{1.33}Ga_{2.66}Ti_{5.34}O_{16}$ to $Cs_{1.33}Ga_{1.33}Ti_{6.67}O_{16}$

Yun Xu,[‡] Mikhail Feygenson,[§] Katharine Page,[§] Lindsay Shuller Nickles,[¶] and Kyle S. Brinkman[†,‡]

[‡]Department of Materials Science and Engineering, Clemson University, Clemson, South Carolina 29634

[§]Chemical and Engineering Materials Division, Oak Ridge National Laboratory, Oak Ridge, Tennessee 37831

[¶]Department of Environmental Engineering and Earth Science, Clemson University, Clemson, South Carolina 29634

Hollandite solid solutions along the A-site compositional range from the pure barium end-member $Ba_{1.33}Ga_{2.66}Ti_{5.34}O_{16}$ to the pure cesium end-member $Cs_{1.33}Ga_{1.33}Ti_{6.67}O_{16}$ have been synthesized using a solid-state reaction technique. The crystal structure of the hollandite across the entire compositional range remained in the *I*4/*m* space group. Structural evolution was resolved by neutron diffraction, total scattering data, and density functional theory calculations. A trend of decreasing thermodynamic stability with smaller tunnel cations was attributed to increased structural distortion observed in the system. In addition, the tunnel cations' local environment was studied in the eightfold coordinated oxygen cavities. Local binding features of the tunnel cations reveals that the hollandite structure can strongly stabilize tunnel cations, even at elevated temperatures up to 500 K.

Keywords: *nuclear waste; density functional theory; hollandite; neutron diffraction; structural*

I. Introduction

Early reports on the development of crystalline ceramic waste forms pointed to a hollandite structure as a potential candidate for the immobilization of alkaline-earth elements such as rubidium (Rb) and cesium (Cs) found in waste streams from nuclear material reprocessing and treatment.[1,2] The hollandite structure was reported to incorporate Cs by insertion into tunnels in the solid resulting in compositions of the form $Ba_xCs_y(Al,Ti)_8O_{16}$.[3] In the absence of Ti^{3+}, Cs substitution for Ba on the A-site of the hollandite structure was limited to 0.3 Cs per unit cell when processed under ambient air. This limitation was believed to be the result of the large size of the Cs ion (R = 1.75 Å), which imposes an unacceptable level of deformation on the $Ba_xCs_y(Al,Ti)_8O_{16}$ hollandite structure. More recently, a number of publications have focused on the compositional ranges of various B-site dopants (i.e., Al, Ga, Fe, Cr, Mg) and their impact on Cs incorporation.[3–6] However, limited studies have reported on the A-site compositional range, especially at high Cs concentrations. One of the potential reasons that high Cs concentrations have not been reported is due to enhanced Cs volatilization at elevated temperatures. Among these various dopants, Ga has demonstrated the ability to lower the melting point and therefore the sintering temperature.[7] A lower sintering temperature is essential in order to reduce the Cs volatilization. In our previous work, Ga-doped pure Cs hollandite has been successfully synthesized in a closed atmosphere, which maintained a high vapor pressure of Cs in the gas phase which limited Cs volatility.[7] The advantage of substituting Ti with Ga. This process is similar to processing routes used to fabricate lead (Pb)-rich ceramics that exhibit similar volatility issues.[8,9] Compositional analysis by inductively coupled plasma mass spectroscopy confirmed all compositions are close to the targeted compositions.[7] X-ray diffraction (XRD) of this high Cs-containing hollandite exhibited the expected *I*4/*m* space group.

The remarkable property of hollandite to incorporate large concentrations of dopants into tunnels of channels without any loss of structural integrity is related to the details of the crystal structure shown in Fig. 1. Metal B-site cations are coordinated in an octahedral fashion by oxygen anions, which are linked via edge and corner sharing oxygen to form a three-dimensional tunnel framework. The A-site elements Ba and Cs occupy the resulting tunnels that form and are coordinated by eight oxygen atoms. The overall hollandite crystal structure and symmetry is determined from the combined effect of the A-site cations, which sit inside the tunnel, and the B-site cations, which control the tunnel geometry. Previous studies have demonstrated that hollandite can adopt a different space group ranging from *I*4/*m* to *I*2/*m* due to differences in the ionic radius of B-site dopants.[10] The transformation from tetragonal to monoclinic occurs when the ionic radii ratio (R_b/R_a) between the octahedrally coordinated cations (R_b) and the tunnel cations (R_a) is higher than 0.48.[11]

The distortion of the octahedral sites have a profound effect on the mobility of cations in the tunnels as discussed in previous studies focused on lithium ion conductors.[12] Another important structural feature pointed out in this work is the displacement of tunnel cations from special positions (2*b*). The ideal hollandite structure is a tetragonal structure with the space group of *I*4/*m*.[11] In this structure, tunnel cations lay on 2*a* Wyckoff positions, the octahedrally coordinated B-site cations are disordered on the 8 h Wyckoff positions, while the oxygen atoms lay on 8 h Wyckoff positions. In the perovskite structure, the tolerance is related to the thermodynamic and structural stability. For instance, the thermodynamic stability is critical for preserving the structural identity of perovskite during applications in catalysis with varying redox cycles of B-site cations used in catalysis which avoid decomposition toward less active single-oxide components.[13,14] A similar argument applies to hollandite-structured materials in nuclear waste immobilization applications. Despite the extensive interest in hollandite materials across a wide range of applications such as catalysis, super ionic conductors, ferromagnetic materials, and nuclear waste forms, there has been little attention paid to the correlation between fundamental thermodynamics and crystal chemistry. The thermochemistry of hollandite based on the formation enthalpies as a function of the average cation radius on the

T. Vanderah—contributing editor

Manuscript No. 38473. Received April 18, 2016; approved July 9, 2016.
[†]Author to whom correspondence should be addressed. e-mail: ksbrink@clemson.edu

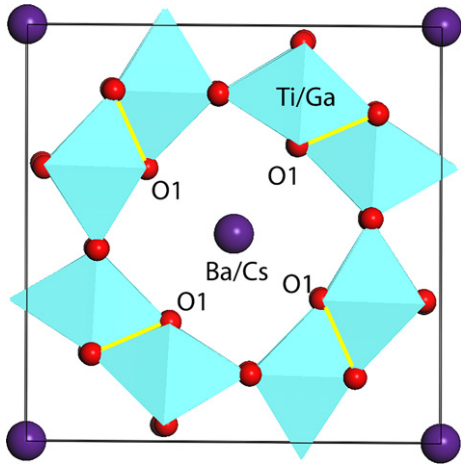

Fig. 1. Representitive of hollandite structure projected along [001] direction.

B-sites[15] has indicated that stability increases with a decreasing average B-site cation radius.[10] This behavior was also observed in pyrochlore-structured materials where the formation enthalpy was more positive as the R_A/R_B ratio decreases, indicating reduced stability of the structure with smaller A-site cations.[16] The decreased stability is also consistent with the observation that pyrochlore has an increasing tendency to transition to a disordered fluorite structure as R_A/R_B decreases.[17] In this work, the thermodynamic stability of hollandite solutions across a wide compositional range will be discussed in terms of structural distortion and symmetry as determined from the temperature-dependent neutron diffraction experiments.

In this study, the hollandite solid solution $(Ba,Cs)_{1.33}(Ga,Ti)_8O_{16}$ across the A-site compositional range was examined. Stoichiometric compositions of hollandite were prepared with a range of B-site compositions (Ga/Ti ratio varied from 0.25 to 0.5) to balance the charge induced by the replacement of Ba^{2+} with Cs^{1+} on the A-site. However, due to the small difference between the ionic radii of Ga (0.620 Å) and Ti (0.602 Å), the solid solution structure largely depends on the A-site atoms. High-resolution neutron diffraction was used to track the evolution of the crystal structure across the A-site compositional range. Based on previous density functional theory (DFT) calculations, we found that by substituting Ba with Cs, the hollandite structure was stabilized as indicated by a decrease in the calculated formation enthalpies.[7] This particular hollandite solution series composition simulates the decay process of hollandite where one Cs is replaced by Ba, and Ga^{3+} is a substituted for reduced Ti^{3+}. In the present work, the stability of the hollandite structure is addressed using neutron diffraction determined structural parameters, bond-valence arguments, and DFT calculations.

II. Experimental Procedure

(1) Synthesis

Hollandite compositions across the A-site solid solution compositional range were synthesized by a solid-state reaction method. All the samples were calcined at 1150°C for 30 h, followed by sintering process at 1250°C for 3 h. A detailed experimental conditions and explanation regarding the selection of compositions can be found in our previous work.[7] The calculated, synthesized, and measured compositions are presented in Table I. Three samples in total were synthesized from Ba end-member ($Ba_{1.33}Ga_{2.66}Ti_{5.34}O_{16}$) to Cs end-member ($Cs_{1.33}Ga_{1.33}Ti_{6.67}O_{16}$). S1, S2, and S3 denote three samples with the composition $Ba_{1.33}Ga_{2.66}Ti_{5.34}O_{16}$, $Ba_{0.667}Cs_{0.667}Ga_2Ti_6O_{16}$, and $Cs_{1.33}$ $Ga_{1.33}Ti_{6.67}O_{16}$, respectively.

(2) DFT Calculations

DFT calculations were performed to determine the minimum energy of the tunnel cations as a function of position for multiple configurations of the Ga/Ti arrangement in the octahedral sites. A total tunnel site occupancy of two-thirds was chosen to generate an integer number of four atoms in the tunnels for the 1 × 1 × 3 supercells. Therefore, the structure consisted of six tunnel sites filled with four Ba^{2+} and/or Cs^+ cations with the Ti^{4+} and Ga^{3+} distributed over the 24 available octahedral cation sites. A basic formula of $(Ba,Cs)_xGa_yTi_{8-y}O_{16}$ was used in the calculations and the Ga/Ti ratio was varied to balance the positive charge induced by the tunnel cations. The electron exchange correlation energy was approximated using the generalized gradient approximation with the Perdew–Burke–Ernzerhoff functional (GGA-PBE)[18] as implemented in Cambridge Serial Total Energy Package (CASTEP).[19] Geometry optimizations were performed to a tolerance of 10^{-6} eV/atom.

(3) Data Collection and Analysis

Time of flight neutron diffraction experiments were performed at the Nanoscale Ordered Materials Diffractometer at the Spallation Neutron Source of Oak Ridge National Laboratory[20] at various temperatures. About 100 mg of powder samples were contained in quartz capillaries. The data were collected in argon atmosphere at 100, 300, and 500 K. The pair distribution function (PDF) function, $G(r)$, was obtained by a Fourier transform of the structure factor, $S(Q)$:

$$G(r) = (2/\pi)\int_{Q=0}^{Q_{max}} Q[S(Q)-1]\sin(Qr)\mathrm{d}Q.$$

where Q is the magnitude of the scattering vector ($Q = 4\pi\sin\theta/\lambda$), 2θ is the scattering angle, r is distance, and λ is the neutron wavelength. The structure factor was obtained from diffraction patterns by subtracting the scattering from the empty container and normalizing by the scattering from a solid vanadium rod. The neutron diffraction data was analyzed using the Rietveld method within the General Structure Analysis System (GSAS) program.[21] Following this procedure, the refined structure from GSAS was used as the initial structure for the refinements of experimental PDF using the PDFGui software package.[22]

III. Results and Discussion

(1) Rietveld and PDF Analysis

The diffraction data collected across the hollandite solid solution range were analyzed using *I*4/*m* symmetries. The structural refinement was performed from neutron powder diffraction data using reported structural parameters for Ba-

Table I. Table of Synthesized and Computed Compositions

Synthesized	$Ba_{1.33}$ $Ga_{2.66}Ti_{5.34}O_{16}$	$Ba_{0.667}Cs_{0.667}Ga_2Ti_6O_{16}$	$Cs_{1.33}$ $Ga_{1.33}Ti_{6.67}O_{16}$
DFT modeled (1 × 1 × 3 super cell)	$Ba_4Ga_8Ti_{16}O_{48}$	$Ba_2Cs_2Ga_6Ti_{18}O_{48}$	$Cs_4Ga_4Ti_{20}O_{48}$
Short name	S1	S2	S3

hollandite ($Ba_{1.24}Al_{2.48}Ti_{5.52}O_{16}$) as the starting model.[15] In the refinement, the Ba and Cs were assumed to be randomly distributed in the tunnel sites. Similarly, the Ga and Ti ions were assumed to be randomly distributed over the octahedral B-sites. Constraints were placed on the occupancies of the A and B-sites to maintain charge neutrality over the unit cell and maintain a total of eight (Ga + Ti) ions at the B-sites. All of the obtained patterns were successfully refined in the *I*4/*m* space group. The final atomic coordinates, unit cell parameters, and discrepancy factors for the refinements in the tetragonal model are given in Table II. Figure 2 displays a typical refinement result of S1 in which the observed data, simulation data, and the difference are plotted.

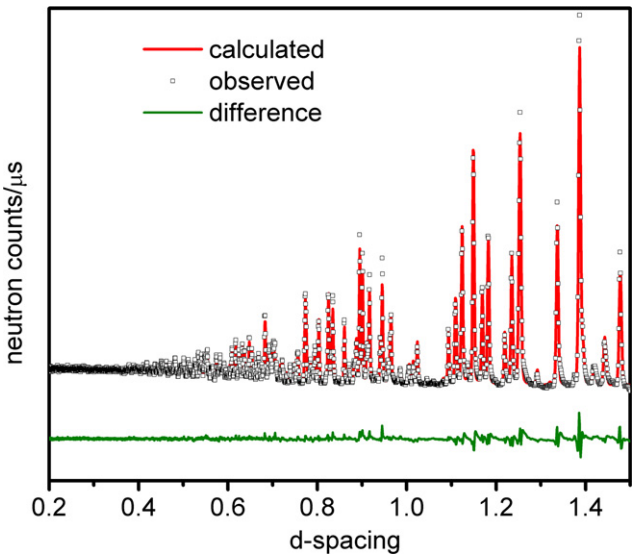

Fig. 2. A representative Time of Flight neutron diffraction and refinement results of S1.

(2) Structural Evolution

(A) Lattice Parameter and Thermal Expansion: The lattice parameters, specifically a (perpendicular to the tunnel direction) and c (parallel to the tunnel direction), are plotted against Cs occupancy as a function of temperature (Fig. 3). As seen from the Fig. 3(a), the a parameter increases as Cs occupancy increases, in contrast to the *c* parameter, which remains relatively constant with increasing Cs occupancy. Upon heating, both the *a* and *c* parameters expand. The cell parameters were fit with a linear regression to obtain the thermal expansion coefficients indicated as the slope (K_a and K_c) in Fig. 3(b). The overall magnitude of the thermal expansion coefficients were similar in value to those reported elsewhere.[15] However, the thermal expansion coefficients calculated from neutron diffraction data in the present case indicate the behavior is not isotropic. This result does not seem to agree with recent reports by Xu et al. where samples of Al-doped hollandite of the form $Ba_{1.17}Al_{2.10}Ti_{5.84}O_{16}$ displayed isotropic expansion.[15]

The thermal expansion coefficient K_a decreases dramatically as the Cs/Ba atomic ratio increases, while the thermal expansion coefficient K_c remains relatively constant. This phenomena agrees with the increased symmetry resulting from increased Cs content. The unique anisotropic thermal expansion is probably related to the differences in the oxygen octahedral edge linkages which form the tunnel structure shown in Fig. 4(a). Oxygen edges that are parallel to the *a*- and *c*-axis are outlined in red specifically in the green circle. Figure 4(b) displays the O–O edge distances of composition S1 plotted as a function of temperature. An examination of the bond distances between different types of O–O revealed different trends observed for the various oxygen edges. The particular O–O edge of O1(2)–O1(2) or O2(2)–O2(2), which are parallel to *c*-axis, and O–O edge O1(2)–O2(2), which is parallel to *a*-axis, show a different extent of elongation with increasing temperature. The temperature dependence of various oxygen distances explains the anisotropic thermal expansion of the framework.

(B) Octahedral Distortion: Characterization of the polyhedral distortion is an essential component to understand the crystal chemistry of the hollandite structure. Many authors have attempted to quantify these deviations from ideality.[23] In the perovskite, pyrochlore and spinel structures, there has been significant discussion regarding the octahedral distortion that leads to a deviation from the ideal cubic or tetragonal structure. An intrinsic origin of this octahedral distortion is cation displacement from the center of symmetry in the structure, which is often due to Jahn–Teller distortion (either compression or elongation of the octahedral as shown on the left of Fig. 5) which removes the degeneracy and lowers the overall energy of system.[24] This usually happens for octahedral complexes with odd number of electrons occupying the e_g orbitals. In our case, there is no degeneracy since Ga^{3+} has a fully occupied *d* orbital and Ti^{4+} has no *d* orbital electrons. The octahedral distortion is due to the displacement of Ga/Ti from their center positions and leads to three long and three short Ga/Ti–O bonds as shown in Fig. 5.

The pair distribution functions of the three hollandite samples (S1, S2, and S3) are displayed in Fig. 6(a), where the inset picture shows significant discrepancies that appear at short distances ($r < 4$ Å). The first peak, centered at around 1.9 Å, is a two component peak, with contributions from all of the Ti/Ga–O peaks. Figures 6(b)–(d) show the fitting results of S1, S2, and S3, respectively. An increase of peak intensity for the Ti/Ga–O from the pure cesium end-member (S3) to the pure barium end-member (S1) suggests the same local environment is found for both Ti and Ga. The Rietveld refinement results indicate that three long M–O bonds and three short M–O bonds exist in the octahedral bonding site. From the calculated PDFs, we determined the r ranges associated with each atomic pair inside the tunnel framework of the hollandite unit cell. For *r* values ranging from 1.6 to 2.4 Å, only the Ti–O or Ga–O pairs in the TiO_6 and GaO_6 octahedral contribute to the PDFs. At the low *r* range of the 1.6–2.4 Å, PDFs of the hollandite series with different Ga/Ti atomic ratios, agree with the Rietveld refinement as shown in Table III. It should be noted that the M–O peaks are negative due to the negative neutron scattering length of Ti. In particular, when the atomic ratio of Ga/Ti is ½ for S1, a peak split was observed with the appearance of a negative peak and a positive peak. With a decreasing Ga/Ti ratio, the

Table II. Unit Cell, Positional, and Reliability Factors for the Refinements of Hollandite Phases in the Tetragonal *I*4/*M* Space Group from Neutron Powder Diffraction Data at 100 K

	Ba/Cs(*z*)	Ti/Ga(*x*)	Ti/Ga(*y*)	O1(*x*)	O1(*y*)	O2(*x*)	O2(*y*)	Rwp (%)
S1	0.432(24)	0.3777(26)	0.145(5)	0.1493(7)	0.1995(6)	0.5418(5)	0.1622(9)	12.6
S2	0.398(0)	0.374(0)	0.171(0)	0.155(0)	0.203(0)	0.541(0)	0.165(0)	6.69
S3	0.333(0)	0.349(15)	0.173(17)	0.157(0)	0.208(0)	0.534(0)	0.167(0)	14.5

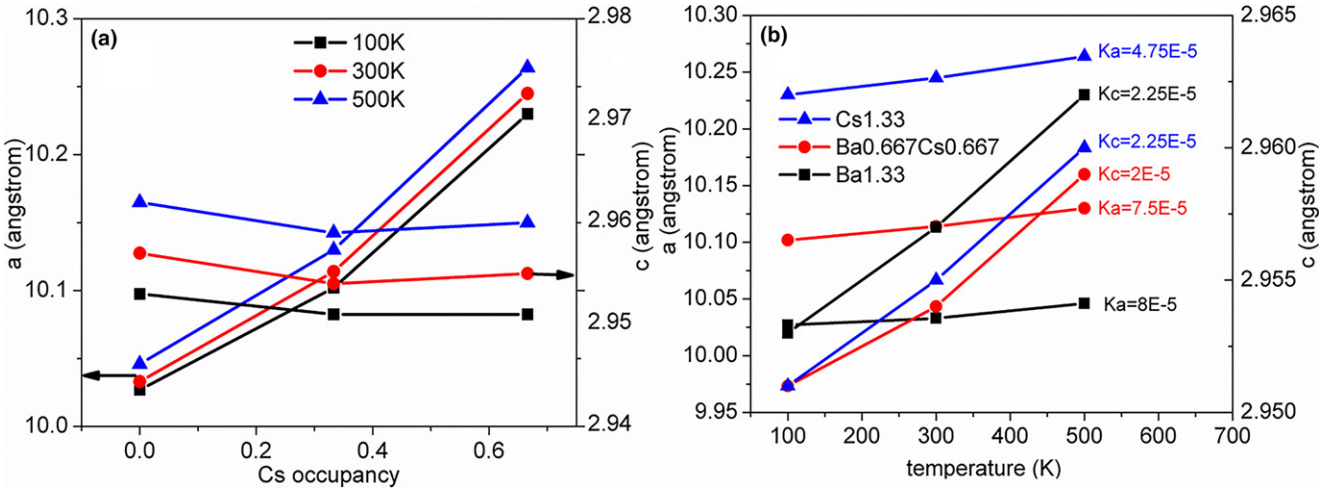

Fig. 3. Evolution of lattice parameters with increasing Cs content and temperature: (a) lattice parameters versus Cs occupancy; (b) lattice parameters versus temperature.

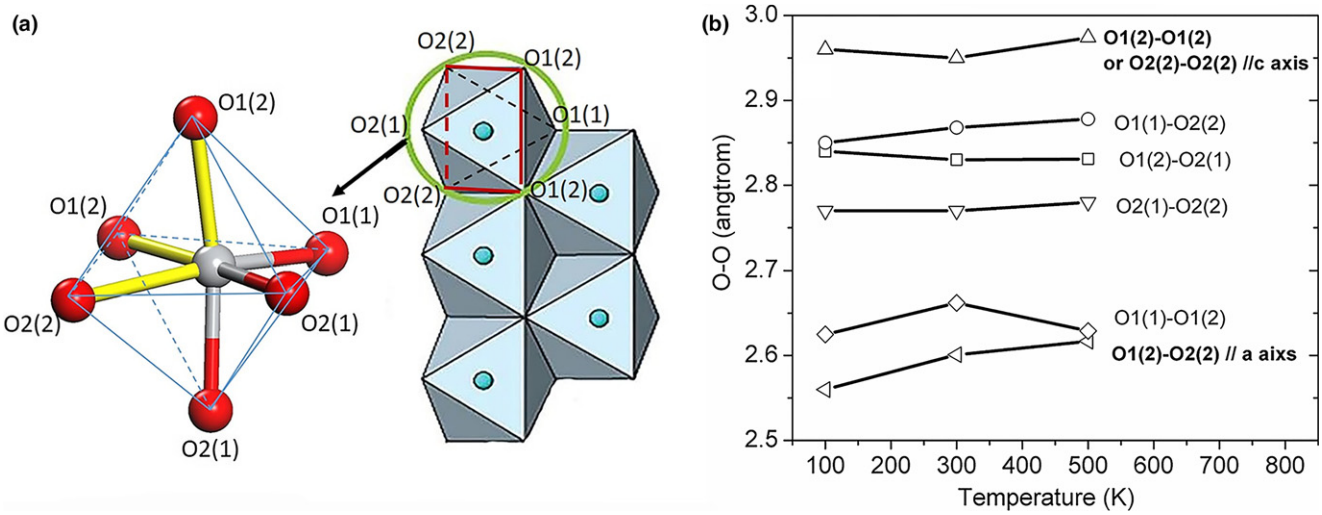

Fig. 4. (a) Schematic of double chain that forms the B-site framework with a single B-site octahedron emphasized to show the arrangement of coordinating oxygen atoms, (b) O–O edges of octahedron evolution with temperature for composition S1.

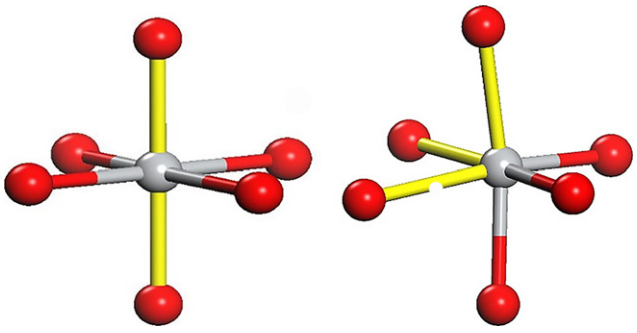

Fig. 5. Representation of octahedral distortion. Yellow bonds and gray bonds are of different lengths. The model on the left is an octahedron with two long/short bonds and four short/long bonds. The model on the right displays an octahedron coordinated with three short bonds and three long bonds.

positive contribution of the Ga–O pairs is compensated by the negative contribution of the Ti–O pairs.

The distortion of octahedron are measured by the distortion parameters proposed by Robinson[25] including DI(M–O), DI(O–M–O), DI(O–O), where DI(M–O), DI(O–M–O), DI(O–O) are bond length deviation, bond angle deviation, and edge length deviation, respectively. The Ti/Ga–O bond lengths diverge with a larger Ba/Cs ratio as indicated by the increasing deviation number (Table III). In another words, the octahedron becomes more distorted as additional charges are placed in the tunnel. Although the XRD patterns of S1 falls into the $I4/m$ space group, the atomic refinement shows that S1 is a metastable tetragonal phase stabilized by the distortion and tilting of the octahedra. The octahedra were distorted in the present case in order to adopt the maximum symmetry. The DFT results further support the PDF analysis, showing similar octahedral distortion in the Ba end-member and decreasing distortion with increasing Cs content (Table IV).

(C) Tolerance Factor and Thermodynamic Stability: The tolerance factor is expressed as:

$$t = \{[(r_A + r_O)^2 - 1/2(r_B + r_O)^2]^{1/2}\}/[\sqrt{3}/2(r_B + r_O)]$$

where r_A, r_B, and r_O represents ionic radius of A-site cations, B-site cations, and oxygen atoms. This tolerance factor describes variations from an ideal crystal structure.[10] As Cs content increases, the tolerance factor t approaches unity as shown in Table V; the framework distortion from the ideal tetragonal structure decreases. Previous DFT calculations[7] of this hollandite compositional series showed a more

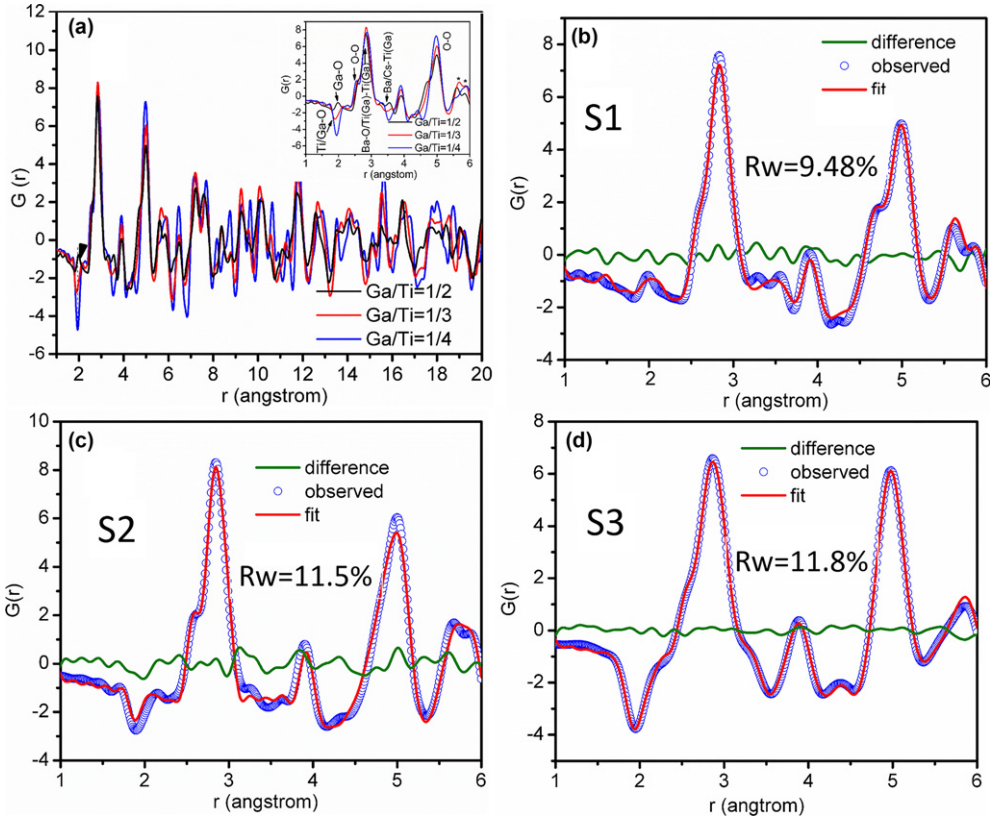

Fig. 6. (a) Atomic pair distribution functions of the hollandite series plotted in a range of 1–20 Å. Inset figure is the zoom in of 1–6 Å with peaks identified. The black line represents the S1 (Ga/Ti = 1/2); the red line represents the S2 (Ga/Ti = 1/3); and the blue line represents the S3 (Ga/Ti = 1/4). Fitting results are displayed G(r) at 100 K for the hollandite solid solutions. Local structure up to 6 A was fit using the structure model from Rietveld refinement.

Table III. Bond Distances Refined from the Diffraction Data Collected at 100 K. Two Different Ti/Ga–O Bonds Exist as Three Short and Three Long Bonds

	Ti/Ga–O1(1)	Ti/Ga–O1(2)	Ti/Ga–O2(1)	Ti/Ga–O2(2)	Ti–O2–Ti	Mean M–O	Deviation
S1	2.18(10)	1.72(9)	1.80(8)	2.25(9)	88.403	1.986	0.46
S2	2.20(13)	1.95(18)	1.71(12)	2.03(19)	93.77	1.978	0.18
S3	2.06(15)	1.92(11)	1.85(13)	2.04(15)	94.116	1.971	0.044

exothermic enthalpy of formation $\Delta H^{\circ}_{f,ox}$ with an increase in the Cs content as shown in Table VI. This implies that a highly symmetric and less distorted hollandite structure results in favorable thermodynamics for phase formation.

(D) Bonding Environment of Ba/Cs in the Oxygen Cavity and Implications for Ba/Cs Immobilization: Ba/Cs is coordinated by eight O(1) atoms, four of which sit above the plane of tunnel cations and four of which are below the tunnel cations plane. The tunnel cations in hollandite can occupy a special position or be displaced along the tunnel toward the four in-plane O atoms with coordinates of (0, 0, 0.5). From the refined positions displayed in Table I, it was found that the Ba atoms were not in the middle of the tunnel, but were displaced toward oxygen plane. This is due to

Table IV. Bond Distances Ti/Ga(M)–O Calculated from Density Functional Theory at 0 K

	Ti/ Ga–O1(1)	Ti/ Ga–O1(2)	Ti/ Ga–O2(1)	Ti/ Ga–O2(2)	Ti–O2–Ti	Mean M–O
S1	2.089	2.131	1.845	1.927	5.066	2.008
S2	1.906	1.989	1.906	2.042	5.312 (Cs)	2.114
					5.553 (Ba)	
S3	1.968	2.019	1.891	2.014	5.515	1.98

Table V. Tolerance Factor for Compositions

Compositions	Mean R_a	Mean R_b	R_b/R_a	Tolerance factor
S1	1.42	0.610	0.429	0.803
S2	1.545	0.6009	0.394	0.875
S3	1.67	0.6079	0.363	0.944

Table VI. Table of Computed Compositions, Associated Experimental Short Name, and Enthalpy of Formation (Calculated for Ga-Hollandite; Measured for Fe-Hollandite)[7,10]

Composition	Short name	Formation enthalpy ΔHf,ox (kJ/mol)	Reference
$Ba_4Ga_8Ti_{16}O_{48}$	S1	−109.6	5
$Ba_2Cs_2Ga_6Ti_{18}O_{48}$	S2	−133.9	5
$Cs_4Ga_4Ti_{20}O_{48}$	S3	−140.8	5
$Ba_{1.24}Fe_{2.48}Ti_{5.52}O_{16}$	–	−223.5 ± 9.1	4

Table VII. Bond Distances Refined from the Diffraction Data Collected at 100, 300, and 500 K. Two Different Kinds of Ba/Cs–O1 Distance Exist

	100 K			300 K			500 K		
	S1	S2	S3	S1	S3	S4	S1	S3	S4
Ba–O1(1)	2.83(16)	2.84(4)	2.85(17)	2.79(6)	2.82 (4)	2.86(16)	2.76(16)	2.87(4)	2.84(6)
Ba-O1(2)	3.06(17)	3.14(5)	3.32(17)	3.15(6)	3.14(5)	3.36(16)	3.17(16)	3.12(4)	3.38(7)
Ba-O2(1)	3.37(9)	3.41(5)	3.45(22)	3.40(8)	3.43(6)	3.43(21)	3.40(22)	3.41(6)	3.43(8)

the stronger electronic interaction between Ba and O compared to Cs and O atoms. As shown in Table VII, refinements showed that the four Ba/Cs–O1(1) bonds were shorter than the four Ba/Cs–O1(2) bonds resulting in a distorted Ba/Cs coordination configuration. Refinement results showed that there are two types of Ba/Cs–Ba/Cs distances, which is due to the existence of vacancies on the A-site, shown schematically in Fig. 7. DFT computations also compared different A-site arrangements. The A–A–V arrangement gives the lowest energy compared to other potential other arrangements This A–A–V arrangement has also been reported in previous studies of the tunnel cation ordering in experimental and computational studies.[26,27] The difference in the displacement is due to the different repulsion forces between adjacent Ba–Ba pairs and Cs–Cs pairs.

An important factor that needs to be addressed in the context of nuclear waste management is whether the Ba or Cs can migrate along the tunnels. The structural features of the oxygen cavity largely determine the potential migration mobility. In the present case, the diagonal oxygen distance O1–O1 should be less than 2 × Ba–O or Cs–O bond distance. Comparing the Ba/Cs–O1 distance and O1–O1 distance which are listed in Table VIII, it should be noted that O1–O1 is always smaller than Ba/Cs–O1 in the hollandite compositional range explored in the present work at temperatures up to 500 K. The local bonding features create a diffusion barrier for the tunnel cations, limiting their mobility.

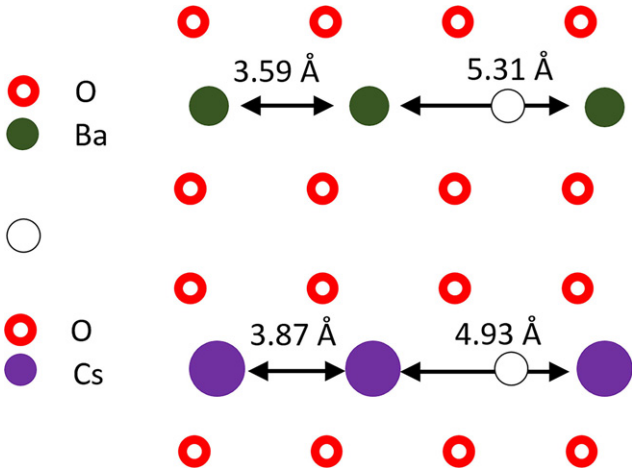

Fig. 7. Representation of the tunnel cations arrangement from side view parallel to [001] tunnel direction.

Table VIII. O1–O1 Distances from PDF Analysis

	500 K	300 K	100 K
S1	5.12	5.08	5.06
S2	5.20	5.18	5.16
S3	5.46	5.36	5.22

IV. Conclusions

The structural evolution and thermodynamic stability of a hollandite solid solution from $Ba_{1.33}Ga_{2.66}Ti_{5.34}O_{16}$ to $Cs_{1.33}Ga_{1.33}Ti_{6.67}O_{16}$ was explored. Since Cs-137, commonly found in high-level waste streams decays to ^{137}Ba, the examination of compositional changes at the A-site simulates the decay process occurring with time for Cs-containing hollandite materials. A higher Cs loading results in a framework expansion in the direction perpendicular to the tunnel axis due to the incorporation of the larger Cs ions, resulting in less distortion in the oxygen octahedra and a more symmetric structure. Higher symmetry structures resulted in a more stable hollandite in terms of formation enthalpy with respect to their constituent oxides. This trend obeys the general rule that increased symmetry results in more favorable phase formation from the thermodynamic viewpoint. Despite increased O–O distance observed with increasing temperature, this value was still small enough to trap the Ba/Cs in the tunnel which is essential for applications as a nuclear waste form. Anisotropic thermal expansion was observed due to intrinsic differences in the O–O edges which form the oxygen octahedral network. Nevertheless, the small value of thermal expansion coefficient observed in this material is beneficial to structural stability. Collectively, these results suggest that hollandite is a promising component of future nuclear waste form immobilization efforts.

Acknowledgments

The research performed at Oak Ridge National Laboratory's Spallation Neutron Source was sponsored by the Scientific User Facilities Division, Office of Basic Energy Sciences, US Department of Energy. The authors gratefully acknowledge financial support from the DOE-EPSCoR Project Number: DE-SC0012530, "Radionuclide Waste Disposal: Development of Multi-scale Experimental and Modeling Capabilities".

References

[1]A. E. Ringwood, S. E. Kesson, N. G. Ware, W. Hibberson, and A. Major, "Immobilziation of Nucleare-Reactor Wastes in Synroc.," *Nature*, **278** [5701] 219–23 (1979).

[2]A. E. Ringwood, S. E. Kesson, N. G. Ware, W. O. Hibberson, and A. Major, "Synroc Process - Geochemical Approach To Nculear Waste Immobilzation," *Geochem. J.*, **13** [4] 141–65 (1979).

[3]V. Aubin-Chevaldonnet, D. Caurant, A. Dannoux, D. Gourier, T. Charpentier, et al., "Preparation and Characterization of (Ba,Cs)(M,Ti)8O16 (M = Al^{3+}, Fe^{3+}, Ga^{3+}, Cr^{3+}, Sc^{3+}, Mg^{2+}) Hollandite Ceramics Developed for Radioactive Cesium Immobilization," *J. Nucl. Mater.*, **366** [1–2] 137–60 (2007).

[4]G. L. F. Bart and H. Rabiller, "Environmental Issues and Waste Management Technologies in the Ceramic and Nuclear Industries IX: Proceedings of the Symposium Held at the 105th Annual Meeting of The American Ceramic Society," *Ceram. Trans.*, **155** [11] 21–9 (2004).

[5]J. Amoroso, J. Marra, S. D. Conradson, M. Tang, and K. Brinkman, "Melt Processed Single Phase Hollandite Waste Forms for Nuclear Waste Immobilization: $Ba_{1.0}Cs_{0.3}A_{2.3}Ti_{5.7}O_{16}$; A = Cr, Fe, Al," *J. Alloy. Compd.*, **584**, 590–9 (2014).

[6]H. Xu, L. Wu, J. Zhu, and A. Navrotsky, "Synthesis, Characterization and Thermochemistry of Cs-, Rb- and Sr-Substituted Barium Aluminium Titanate Hollandites," *J. Nucl. Mater.*, **459**, 70–6 (2015).

[7]Y. Xu, R. Grote, J. Amoroso, L. S. Nickles, and K. Brinkman, "A-Site Compositional Effects in Ga-Doped Hollandite Materials of the Form BaxCsyGa2x + YTi8-2x-YO16: Implications for Cs Immobilization in Crystalline Ceramic Waste Forms"; Scientific Report, 6 27412, 2016.

[8]K. Brinkman, M. Cantoni, D. Su, and N. Setter, "Processing and Properties of Ferroelectric Relaxor Lead Scandium Tantalate Pb(Sc1/2Ta1/2)O3 Thin Films," *J. Mater. Res.*, **22**, 217–32 (2007).

[9]F. Chu, I. M. Reaney, and N. Setter, "Role of Defects in the Ferroelectric Relaxor Lead Scandium Tantalate," *J. Am. Ceram. Soc*., **78** [7] 1947–52 (1995).
[10]G. C. C. Costa, H. Xu, and A. Navrotsky, "Thermochemistry of Barium Hollandites," *J. Am. Ceram. Soc*., **96** [5] 1554–61 (2013).
[11]J. E. Post, R. B. Von Dreele, and P. R. Buseck, "Symmetry and Cation Displacements in Hollandites: Structure Refinements of Hollandite, Cryptomelane and Priderite," *Acta. Cryst. B*, **38** [4] 1056–65 (1982).
[12]T. Zhang, D. Li, Z. Tao, and J. Chen, "Understanding Electrode Materials of Rechargeable Lithium Batteries via DFT Calculations," *Prog. Nat. Sci.: Mater. Int*., **23** [3] 256–72 (2013).
[13]A. Ladavos and P. Pomonis, "Methane Combustion on Perovskites"; pp. 367–88 in *Perovskites and Related Mixed Oxides*, Edited by P. Granger, V. I. Parvulescu, S. Kaliaguine, and W. Prellier. Wiley-VCH Verlag GmbH & Co. KGaA, Weinheim, 2016.
[14]F. Calle-Vallejo, J. I. Martínez, J. M. García-Lastra, M. Mogensen, and J. Rossmeisl, "Trends in Stability of Perovskite Oxides," *Angew. Chem. Int. Ed*., **49** [42] 7699–701 (2010).
[15]H. Xu, G. C. C. Costa, C. R. Stanek, and A. Navrotsky, "Structural Behavior of Ba1.24Al2.48Ti5.52O16 Hollandite at High Temperature: An In Situ Neutron Diffraction Study," *J. Am. Ceram. Soc*., **98** [1] 255–62 (2015).
[16]K. B. Helean, S. V. Ushakov, C. E. Brown, A. Navrotsky, J. Lian, et al., "Formation Enthalpies of Rare Earth Titanate Pyrochlores," *J. Solid State Chem*., **177** [6] 1858–66 (2004).
[17]S. E. Kesson and T. J. White, "Radius Ratio Tolerance Factors and the Stability of Hollandites," *J. Solid State Chem*., **63** [1] 122–5 (1986).
[18]J. P. Perdew, K. Burke, and M. Ernzerhof, "Generalized Gradient Approximation Made Simple," *Phys. Rev. Lett*., **77** [18] 3865–8 (1996).
[19]M. C. Payne, M. P. Teter, D. C. Allan, T. A. Arias, and J. D. Joannopoulos, "Iterative Minimization Techniques for ab Initio Total-Energy Calculations: Molecular Dynamics and Conjugate Gradients," *Rev. Mod. Phys*., **64** [4] 1045–97 (1992).
[20]J. Neuefeind, M. Feygenson, J. Carruth, R. Hoffmann, and K. K. Chipley, "The Nanoscale Ordered MAterials Diffractometer NOMAD at the Spallation Neutron Source SNS," *Nucl. Instrum. Methods Phys. Res., Sect. B*, **287**, 68–75 (2012).
[21]A. C. Larson and R. B. Von Dreele, "General Sturcutre Analysis System"; LA-UR 86-748, 1994.
[22]C. L. Farrow, P. Juhás, J. W. Liu, D. Bryndin, E. S. Bozin, et al., "PDFgui User Guide"; 2007.
[23]R. M. Hazen, R. T. Downs, and C. T. Prewitt, "Principles of Comparative Crystal Chemistry," *Rev. Mineral. Geochem*., **41** [1] 1–33 (2000).
[24]H. A. Jahn and E. Teller, "Stability of Polyatomic Molecules in Degenerate Electronic States. I. Orbital Degeneracy," *Proc. R. Soc. Lond A Math. Phys. Eng. Sci*., **161** [905] 220–35 (1937).
[25]K. Robinson, G. V. Gibbs, and P. H. Ribbe, "Quadratic Elongation: A Quantitative Measure of Distortion in Coordination Polyhedra," *Science*, **172** [3983] 567–70 (1971).
[26]J. Vicat, E. Fanchon, P. Strobel, and D. Tran Qui, "The Structure of $K_{1.33}Mn_8O_{16}$ and Cation Ordering in Hollandite-Type Structures," *Acta Crystallogr. Sect. B*, **42** [2] 162–7 (1986).
[27]A. Pring, D. J. Smith, and D. A. Jefferson, "Supercell Ordering in a Hollandite-Type Phase: Potassium Magnesium Antimony Oxide," *J. Solid State Chem*., **46** [3] 373–81 (1983). □